A tool for designing tree-like concentration gradient generators for lab-on-a-chip applications

Milad Ebadi [a], Khashayar Moshksayan [a,1], Navid Kashaninejad [b,1], Mohammad Said Saidi [a,*], Nam-Trung Nguyen [b,*]

[a] Department of Mechanical Engineering, Sharif University of Technology, Tehran 11155, Iran
[b] Queensland Micro- and Nanotechnology Centre, Griffith University, Nathan Campus, 170 Kessels Road, Brisbane, QLD 4111, Australia

HIGHLIGHTS

- TCDT can be used to find CGG dimensions.
- TCDT calculates non-linear output concentrations based on the flow at the inlets.
- TCDT is ready-to-use for three different CGG microchips.
- Food dye is more efficient than fluorescent intensity measurement for multidrug.
- MDMC method can be used to find the best concentration for combinatorial drug tests.

ARTICLE INFO

ABSTRACT

Concentration gradient generators (CGGs) help biologists to perform large scale, fast and high-throughput experiments. This paper introduces a design tool called Tree-like Concentration gradient generator Design Tool (TCDT). The performance of this tool is validated both numerically and experimentally. Three CGGs were fabricated using three different fabrication methods and design parameters. The performance of these devices was examined using the measurement of fluorescent and dye intensity. The performance of the design tool for non-linear and multi-drug concentration gradient generations was investigated as well. In addition, a method was developed to investigate the multi-drug concentration effect, which can be the starting point for off-the-shelf usage of the CGGs in personalized medicine. Experimental data, as well as numerical results, confirmed that the output concentrations of the CGGs were within five percent of the values predicted by the design tool. This open-source software is available online for public use.

© 2019 Elsevier Ltd. All rights reserved.

1. Introduction

In most biosynthesis activities, concentration of chemicals significantly affects cellular behavior (Hu et al., 2017). The transfer of gases from cells to the environment is completely dependent on the concentration gradient of the gases in the environment and within the tissue (Truskey et al., 2004). Various phenomena in the body such as cell division and cellular movement (Chung et al., 2005; Huang et al., 2017; Lee et al., 2011; Park et al., 2007), immune function (Joanne Wang et al., 2008; Kothapalli et al., 2011), wound healing (Wang, 2009), tumorigenesis (Chiang et al., 2012), and osteogenesis (Heo et al., 2010) are closely related to the concentration gradient of the species within the tissue. In cancer medications, an optimized concentration of a drug should be used for patients to achieve the best outcome. Therefore, for each patient, different concentrations of the drug should be tested first, and the best dose needs to be applied later (Ruppen et al., 2015). For this reason, different methods have been developed to generate concentration gradients.

Concentration gradient generators (CGGs) are among the most efficient devices employed for precise generation of various concentration gradients. In this context, concentration gradients refer to the concentration output of the device with a predictable distribution. Advances in microtechnology, particularly in microfluidics, enhances the design and function of CGGs significantly. These

* Corresponding authors.
    E-mail addresses: mssaidi@sharif.edu (M.S. Saidi), nam-trung.nguyen@griffith.edu.au (N.-T. Nguyen).
    [1] These authors contributed equally to this work.

enhancements have been generally attributed to the reduction of the dimensions of the device. Methods for generating concentration gradients in CCGs can be grouped in four categories: membrane methods (Boyden, 1962; Zicha et al., 1991; Zigmond SH, 1973), micro pipetting (Gundersen and Barrett, 1979), serial dilution (integra_support, 2017), and microfluidic methods (Abhyankar et al., 2006; Bui et al., 2011; Huang et al., 2017; Kilinc et al., 2016; Nguyen et al., 2016).

Microfluidic CGGs have emerged as essential components in most cell culture and organ-on-a-chip platforms (Kashaninejad et al., 2016; Moshksayan et al., 2018a; Moshksayan et al., 2018b). Microfluidic CGGs divide into subgroups such as the diffusion-based method (Abhyankar et al., 2006), pressure balance (Kilinc et al., 2016), T-junction (Bui et al., 2011), hydrogels (Nguyen et al., 2016), and tree-like CGGs (Huang et al., 2017).

Tree-loke CGGs are frequently used for drug screening in microfluidic cell culture platforms because they can generate more precise and stable concentrations (Chang et al., 2014b; Diao et al., 2006; DiCicco and Neethirajan, 2014; Hong et al., 2016; Huang et al., 2017; Jang et al., 2011; Jeon et al., 2000; Keenan and Folch, 2008; Kothapalli et al., 2011; Lee et al., 2010; Nguyen et al., 2016; Park et al., 2007; Tretkoff, 2005; Ye et al., 2007). Moreover, this subgroup is easier to use and more robust against variations in environmental conditions (Jeon et al., 2000). One of the first attempts to design tree-like CGGs was reported by Jeon et al. (2000). The authors designed a tree-like CGG based on an analytical model of concentration and pressure. The flow rate was 50 μl/min, and the dimension of the channel was 50 μm, both in width and height. The generated concentration was precise and stable near the design flow rate. However, the output concentration deviated from the predicted values at higher flow rate. This research was a reference for most of the subsequent studies on CGGs (Huang et al., 2017; Jeon et al., 2002; Jin et al., 2016; Lim and Park, 2018; Lin et al., 2004; Walker et al., 2005).

Different tree-like CGGs can generate non-linear concentration gradients. However, the most common approach is using different inlet flow rates because of the low cost and simple implementation (Toh et al., 2014). Lin et al. designed tree-like CGGs with multiple inlets to generate non-linear concentration gradients (Lin et al., 2004). The devices created logarithmic and exponential profiles. A non-linear concentration gradient can be generated with other concepts such as electroosmosis (Glawdel et al., 2009; Jain et al., 2010), which besides fluid pumping can also concentrate charged particles. This method has biochemical and environmental applications. Nevertheless, channel clogging is a major challenge associated with this method. Several attempts have been made to solve the clogging issue. For instance, Harrison et al. presented a method for preconcentration of polystyrene particles and E.coli cells in a low-conductivity medium (Harrison et al., 2015). Ren et al. studied effective electrokinetic enrichment of fluorescent polystyrene nanoparticles on ideally polarizable metal strips using hybrid electroosmotic kinetics as bi-phase induced-charge electroosmosis (BICEO) with a four-terminal spiral electrode array (Ren et al., 2019). Liu et al. developed a reliable method for flexible regulation on the spatial-temporal evolution of ion-depletion layer by electroconvective mixing (Liu et al., 2019).

Another application of tree-like CGGs is generating multi-drug concentration gradients. Liu et al. designed a multilayer CGG using the monolithic fabrication method (Liu et al., 2008). Their device could generate various combinations such that three drugs were mixed equally or each pair of the drugs existed with the same concentration. Lee et al. designed another CGG using rapid prototyping method that could generate multiple concentration gradients of one or more species based on the number of layers of the chip (Lee et al., 2010). The fabrication of both devices was complicated and expensive. Another creative design using multi-drugs in the

experiment was performed by Yang et al. (2011). The authors introduced a circular design in the orientation of the output channels to generate a single layer chip for cell apoptosis and multi-drug drug screening.

Designing tree-like CGGs is a complex procedure and needs in-depth knowledge of mass transport and fluid dynamics. Thus, most researchers prefer to adopt their designs from previously reported devices to bypass the tedious procedure (Chang et al., 2014a; DiCicco and Neethirajan, 2014; Huang et al., 2017; Jin et al., 2016; Toh et al., 2014). In a previous work (Rismanian et al., 2019), we introduced a dimensionless number, which is constant for each type of CGG. This number is useful for designing mixers but cannot model the entire CGG because it does not consider the connecting channels and the different flow rates. Depending on the flow rate and the material used in the device design, design parameters such as channel width, mixers' length, culture media, and cells are unique for each application. Therefore, this study uses the analytical model of concentration, and a simple procedure was developed to facilitate the design of CGGs with minimum knowledge of the physics of CGGs and engineering principles.

This paper reports a novel Tree-like Concentration gradient generator Design Tool (TCDT) based on the fluid mechanics' models and previous research on CGGs. By using this tool, researchers can customize tree-like CGGs based on the required flow rate, fabrication method, material, and dimensions. The validity of the tool was evaluated using both computational fluid dynamics (CFD) simulations and experimental investigation for three different tree-like CGGs, each of which was fabricated by a different method. Furthermore, we report a method for examination of multi-drug screening based on Yang's design of CGGs (Yang et al., 2011). Yang's approach with slight modifications could serve as of-the-shelf usage of the CGGs for personalized medicine (Mark et al., 2012). The method finds the best concentration of the drug for each person, reducing side-effects as well as increasing the effectiveness of the drug (Ruppen et al., 2015). The verifications of the output concentrations were based on the Rhodamine-B diffusion coefficients. TCDT executable file has been uploaded on the following link (https://github.com/Biofluidmechtools/TCDT.git) for public use, and the source code is available on demand.

2. Materials and methods

2.1. The architecture of the tree-like concentration gradient generator design tool

The Tree-like Concentration gradient generator Design Tool (TCDT) uses the corrected mathematical model that will be explained in the upcoming sections to estimate the device performance. The required information for the user is the fabrication method, the required flow rate, diffusion coefficient, dimension constraints, maximum shear stress on the wall, and other fabrication and material constraints that the user provides as input for the design (Fig. 1A). The detailed information needed to design the device and the manual of the tool are reported in the ESI.

2.2. Mathematical model

Tree-like CGGs produce the concentration gradient in the presence of flow. Because at low velocities and small dimensions, the Reynolds number is on the order of unity leading to laminar flow in most cases (Keenan and Folch, 2008). In a low-Reynolds-number laminar flow, mixing occurs through diffusion and convective mass transfer (Shames, 2003). Therefore, the channels should be sufficiently long to facilitate proper diffusive mixing (Çengel, 2010). The mathematical model is based on the analytical solution
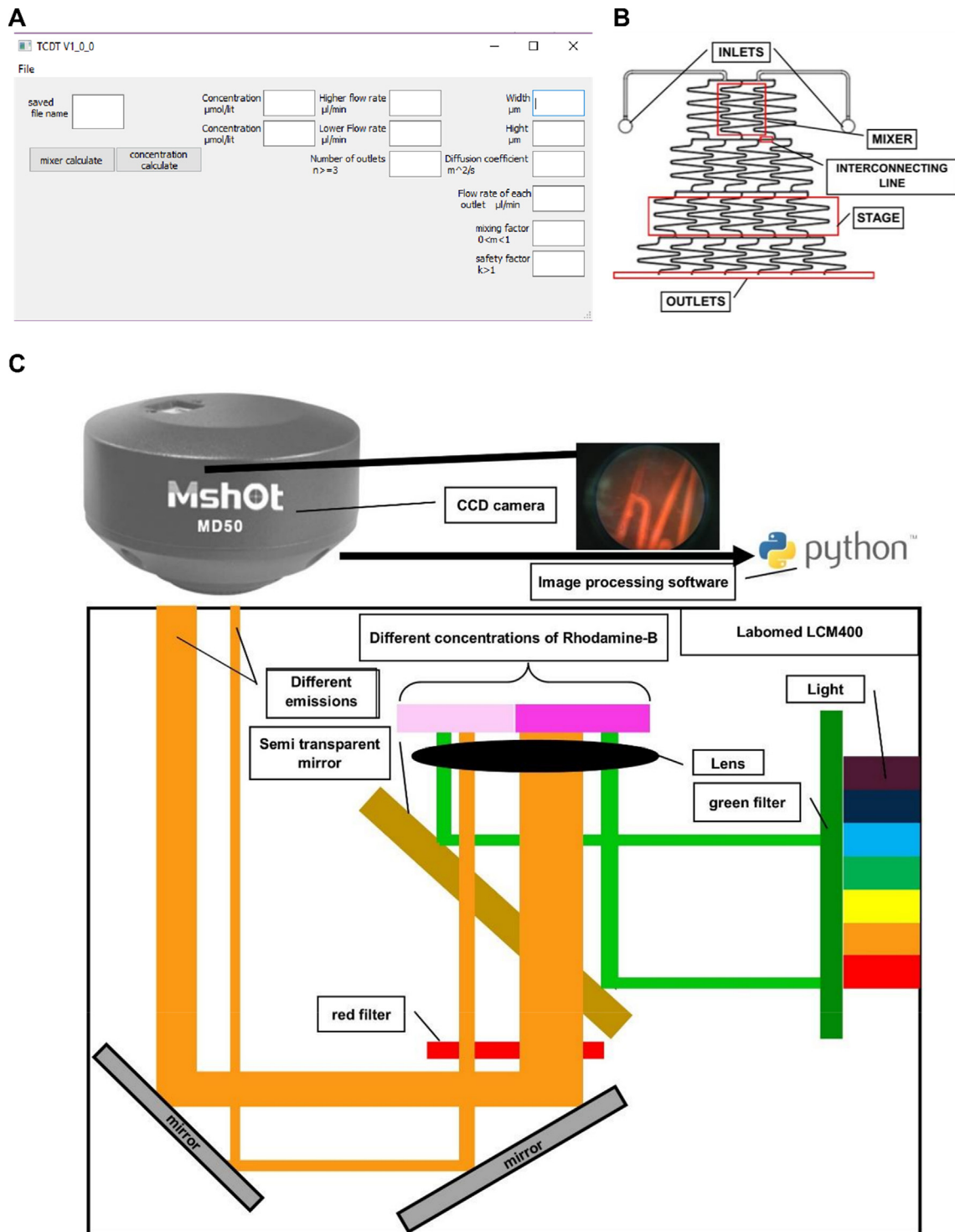
Fig. 1. (A) The user interface of the design tool. (B) Schematic representation illustrating different parts of the device. (C) Schematic of concentration measurement system.

of the flow and the analytical diffusion model of two parallel flows in a rectangular channel.

2.3. Fluidic-electric analogy

CGGs are made from some similar blocks of mixers that have the same fluid dynamic properties. Each mixer could be modeled as a resistor and the CGG as an electric circuit. Using this method (Eq. (1)), the flow is analogous to electric current, and the pressure

drop is analogous to electric voltage difference (Eq. (2)). With this method, the resistance and the flow rate in each mixer can be found (Nguyen, 2012a).

$$\Delta P = R_f Q \qquad (1)$$

$$R_f = 3\mu L \left(a^3 b \left(1 - \frac{192a}{\pi^5 b} \sum_{n=1}^{\infty} \frac{\tanh\left((2n-1)\frac{b\pi}{2a}\right)}{(2n-1)^5} \right) \right)^{-1} \qquad (2)$$

In Eq. (1), R_f is the channel resistance and, ΔP and Q are the pressure drop and the flow rate of the channel, respectively. In Eq. (2), μ is the fluid viscosity, L is the length of the channel, and a is the width of the rectangular channel.

One of the capabilities of the tree-like CGGs is generating non-linear concentration gradients by introducing different flow rate ratios in each inlet (Fig. 1B). The flow rate ratio for the desired distribution of the output concentration can be calculated using the above fluidic-electric analogy. The flow rate of each mixer (i.e., curved channels that bend continuously and is the part where the mixing effect takes place, Fig. 1B) can be calculated using the pressure drop over each mixing channel. The output concentrations can be calculated using the values of inlet flow rates and concentrations of each mixer. Thus, the flow rate of each mixer and the input concentration determines the output concentration using the conservation of mass from the first stage (Fig. 1B) to the last stage of the device. The mixers, which are located between the same connecting microchannels (Fig. 1B), have the same pressure drop. For linear gradients, all mixers in one stage have the same fraction of the fluid flow of each inlet. Therefore, the flow of each mixing channel could be measured by dividing the total flow rate to the number of mixers in each stage. Each outlet concentration is the linear interpolation of the inlet concentrations. For the devices with nonlinear output, the flow of each mixer should be calculated using the fluidic-electric analogy (Jeon et al., 2000).

2.4. Concentration model

As discussed in the previous section, the fluidic-electric analogy can only determine the discharge rate, which provides the output concentration under the assumption of complete mixing. This method fails to provide any information about the quality of mixing between the two substances. To address this limitation, the length and width of each stage of the device should be appropriately designed to facilitate complete mixing. Accordingly, a new model for the diffusion of two substances in the device's channels was provided. The diffusion of the two low concentration solutions follows the mass transfer equation (Eq. (3)) (Crank, 1979).

$$\nabla \cdot \left(\vec{u} C \right) = D \nabla^2 C \tag{3}$$

In Eq. (3), u is the velocity of the fluid, C is the concentration of the species and D is the diffusion coefficient of the species. The significant part of the diffusion between the two solutions occurs in the mixing channels. Therefore, the diffusion between the two parallel flows in the channels was simulated before designing the mixers. First, the Péclet number (Pe) [$Pe = ul/D$, where l is the characteristic length of the CGG (width of the channel)] should be calculated to determine the dominant mixing mechanism between convection and diffusion. For concentration gradient applications, the highest velocity in a microchannel is about $u = 10$ cm/s (Nguyen, 2012b). The mass diffusion coefficient for Rhodamine-B in a culture medium is $D = 4 \times 10^{-10}$ m^2/s (Toh et al., 2014). The characteristic length for the micro-channels of CGGs, l, is 50 to 100 μm (Gao et al., 2012; Hong et al., 2016; Huang et al., 2017; Jeon et al., 2000; Jin et al., 2016; Lin et al., 2004; Walker et al., 2005). With the above typical values, the Peclet number Pe, with respect to longitudinal velocity and diffusion normal to velocity, is between 1,250 to 25,000. Because of the relatively high Pe, the convection term in the equation is significant. We need to consider the following assumptions to solve the equation. First, by assuming a high aspect ratio microchannel ($H \gg W$, where H and W are height and width of the channel, respectively), the diffusion terms become negligible along the y and z directions, where y and z are the positions along the height and the length of the mixer, respectively. Second, we assume a constant and fully developed one-directional velocity profile in the channel. With these assumptions, the solution of the concentration model becomes as follows (Crank, 1979).

$$C(z,x) = C_0 \left\{ \frac{1}{2} + \frac{2}{\pi} \sum_{n=1}^{\infty} \frac{1}{n} \sin\left(\frac{n\pi}{2}\right) \cos\left(\frac{n\pi x}{W}\right) \exp\left(\frac{-Dn^2\pi^2 z}{\bar{u} W^2}\right) \right\} \tag{4}$$

In Eq. (4), C is the concentration, C_0 is the inlet concentration, x is the position along the width of the mixer, D is the diffusion coefficient, $\bar{u}$ is the average flow velocity, and W is the width of the channel.

We need to consider Dean number (De) to validate the assumption of a fully developed flow. The Dean number is the ratio of the centrifugal forces to inertial forces and for conventional channels, and is the product of the Reynolds number (Re) and square root of the curvature of the channel (Eq. (5)) (Nguyen, 2012a).

$$De = Re\sqrt{\frac{a}{R}} \tag{5}$$

where a is the hydraulic diameter of the channel, and R is the radius of the curvature in the channel. For Dean number less than 40, the effect of the curvature is negligible (Ligrani, 1994). Nevertheless, for conventional CGG designs, the curvature radius is on the order of a millimeter, and the width of the channels is on the order of tenth of millimeters. The Reynolds number is on the order of one. Thus, the Dean number is far below 40 in our case. The flow stays fully developed for all channel lengths, because the inertial effects are dominant over the centrifugal effects. These assumptions are invalid, if the height and the width of the channel are of the same order of magnitude, i.e., for $H \approx W$. In that case, one must optimize the governing equations and the models using CFD optimizations.

2.5. CFD model

The three-dimensional (3D) model of the device was generated in a CAD tool. The device was modeled using a customized CFD code for validating and improving the mathematical model. The mathematical model was improved using optimization techniques (Rao, 1996) to minimise the effects of assumptions mentioned in Section 2.4. Our model was formulated laminar flow with diluted species in high-aspect-ratio channels. The solvent was water, and the solute was the desired material with a diffusion coefficient between 5×10^{-9} and 5×10^{-11} m^2/s (Gendron et al., 2008; Kendig, 2003). The channels were 50 μm in height and 200 μm in width. To certify that the solution was correct, grid independency analysis was performed.

2.6. Soft lithography

The devices were fabricated by standard polydimethylsiloxane (PDMS) soft lithography from the fabricated molds. The molds were washed using deionized (DI) water and isopropanol before soft lithography to remove all the dust. For the positive molds (3D-printed and micromachined molds), PDMS pre-polymer and the curing agent (Silgard 184, Dow Corning, Midland, MI, USA) were mixed in the W/W ratio of 10:1 and poured onto the molds followed by degassing in a vacuum chamber. The mixture was then crosslinked in an oven at 70 °C for 4 h. Subsequently, the PDMS substrate was peeled off the mold, its edges were cut, and the inlets and outlets were punched using a 1-mm biopsy puncher.

For the negative molds fabricated with the photolithography method, PDMS double molding was utilized according to the method developed by Kwapiszewska et al. (Kwapiszewska et al., 2016). Briefly, after going through the above procedure, the PDMS substrate was kept in the oven at 100 °C for 48 h for thermal aging (Kwapiszewska et al., 2016). Then, the PDMS substrate was used as

a positive mold to fabricate the final PDMS device. The final PDMS parts were then bonded to glass substrates. Prior to plasma bonding, the glass substrates were washed with water and detergent and then with DI water and isopropanol.

2.7. Mold fabrication method

We used micromachining, 3D printing, and photolithography for making the mold. Micro milling was used for the fabrication of a positive mold on a Poly(methyl methacrylate) (PMMA) using a computer numerical control (CNC) milling machine (Seiko CNC Inc., Tokyo, Japan). A 0.4 mm CNC cutting tool was used to fabricate the device mold.

For 3D printing, a stereolithography printer Form2 (Formlabs Inc, Somerville, Massachusetts, United States) was used to fabricate the positive mold. The device has a minimum feature size of 150 μm. In order to make the design compatible with the fabrication method, the distance between the channels was chosen to be larger to prevent the fluid within the channels from leaking into each other.

For photolithography, a negative mold was patterned on a silicon wafer using SU8-2050 negative photoresist (MicroChem Co., Newton, MA, USA). Briefly, 4 ml of the photoresist was poured on a 4-inch silicon wafer followed by spin coating by Spin Coater ET-SC-V1 (SATEECO Inc., Tehran, Iran) according to the manufacturer's protocol to achieve a 50-μm thick photoresist film. Then, the soft bake was carried out at 65 °C and 95 °C for 3 min and 9 min, respectively. Subsequently, the photoresist was placed under a UV exposure with a dose of 160 mJ/cm^2 using a mask aligner ET-MA-V1 (SATEECO Inc., Tehran, Iran) and a plastic mask. The coated wafer was then placed on a hot plate for the post-exposure bake (2 min of 65 °C and 10 min of 95 °C) and was developed.

2.8. Concentration measurement

In order to measure the output concentration of the devices, two image processing-based methods were used, namely, the fluorescence intensity measurement and food dye intensity measurement. The images were taken by an MD-50, CMOS camera (Micro-shot Technology Limited, Guangzhou, China), using an LCM400 inverted microscope and florescent module (Labomed. Inc, Los Angeles, USA). The flow was pumped into the device using an EH-003 syringe pump (SATEECO Inc, Tehran, Iran). 1-ml insulin syringes and 2 mm Teflon tubes were used for flow injection at the inlet.

2.8.1. Fluorescence intensity measurement

The fluorescence emission intensity measurement was done using Rhodamine-B (Fig. 1C) and the fluorescence intensity was processed using the Python software (Python, 2019). To quantify the intensity of the fluorescent light for each output concentration in each test, a grayscale image algorithm was developed, in which each image is a light intensity matrix of image pixels (Girod et al., 1999). For each output concentration, three outputs were taken with a time interval of 5 min. Finally, the results of each experiment were processed by evaluating the median value of the grayscale intensity of each photo and the median value of the three images. To overcome the dark noise in the images, their intensity matrices were normalized to the intensity of the highest and lowest intensity of the fluorescence substance in each experiment. In order to validate the results, the desired concentrations were generated manually and measured using the same equipment and algorithms. The predicted concentration in each case was manually generated using conventional method of mixing by a micropipette, to show the effectiveness of the measurement technique. The

mixture was then injected into the device, and the photos were taken under the same conditions of the experiments. Subsequently, the results of those measurements are labeled as "hand made" in Figs. 4F, 5A, and 8D.

2.8.2. Food dye intensity measurement

To measure the concentration using food dye intensity measurement method, red, blue, and yellow food dyes (TEIF Food Inc., Tehran, Iran) were introduced into the chip, and the images were taken from the outlets of each of the device. A customized code was generated in Python to determine the concentration of the output fluid based on the RGB (red, green, blue), Grayscale and HSV (hue, saturation, value) methods. In the HSV method, the image is a matrix whose arrays contain three values indicating the hue, saturation, and value (Girod et al., 1999). This method of representing the color matrix helps measure the color regardless of the light intensity on the sample (Girod et al., 1999).

The hue of the output was determined using the color image matrix. Subsequently, by normalizing color image matrices to the highest and the lowest hue in each experiment branch, the color of each output was identified. Using this method, the dark noise was minimized in the image. Another advantage of this method is improving the quality of the results by omitting the effect of imaging angles and brightness (Ramesan et al., 2016). Similarly, for this method the "hand made" concentration was also generated to examine the accuracy of the measurement technique.

3. Results and discussion

We studied the mixing performance of three CGGs to validate the proposed model. The actual output concentration of each inlet was compared with the predicted output concentration based on the proposed numerical simulation. For each case, the device mold was fabricated using a different fabrication method. The TCDT was used to design these three cases, and the output geometries were used for the subsequent fabrication.

3.1. First case – four-output concentration

The first device under investigation is a CGG that receives single drug and diluter and gives four different drug doses at the outlets (Fig. 2A). The chip mold was fabricated using 3D-printing as mentioned previously. For this chip, the mixing performance was evaluated by measuring the fluorescence emission at each outlet followed by the comparison with the numerically simulated outlet concentration.

The chip was designed based on an input flow rate of 1.25 μl/min for each outlet, resulting in an overall flow rate of 5 μl/min. The dimension of all the microchannels was 40 μm in height and 150 μm in width, set based on the best resolution of the 3D-printer, the datasheet-recommended design points and the analytical model of the device. The design and simulation were carried out based on the diffusion coefficient of 5×10^{-10} m^2/s, which is lower than most of the conventional drugs and diluters commonly used in CGGs (Toh et al., 2014). Grid study was performed and achieved mesh independency (Fig. 2C) using 5.8×10^6 unstructured tetrahedral elements. Fig. 2D shows the representative results of the numerical simulation of the device. The output concentration of the device deviates from the designed value using corrected form of Eq. (4) (labeled as "analytic model" in the figure), if the flow rate exceeds the design value of 5 μl/min because of incomplete mixing.

The performance of the device was experimentally evaluated for different flow rates. As shown in Fig. 2E, the output concentration of the device obeys the simulation results for the flow rate of
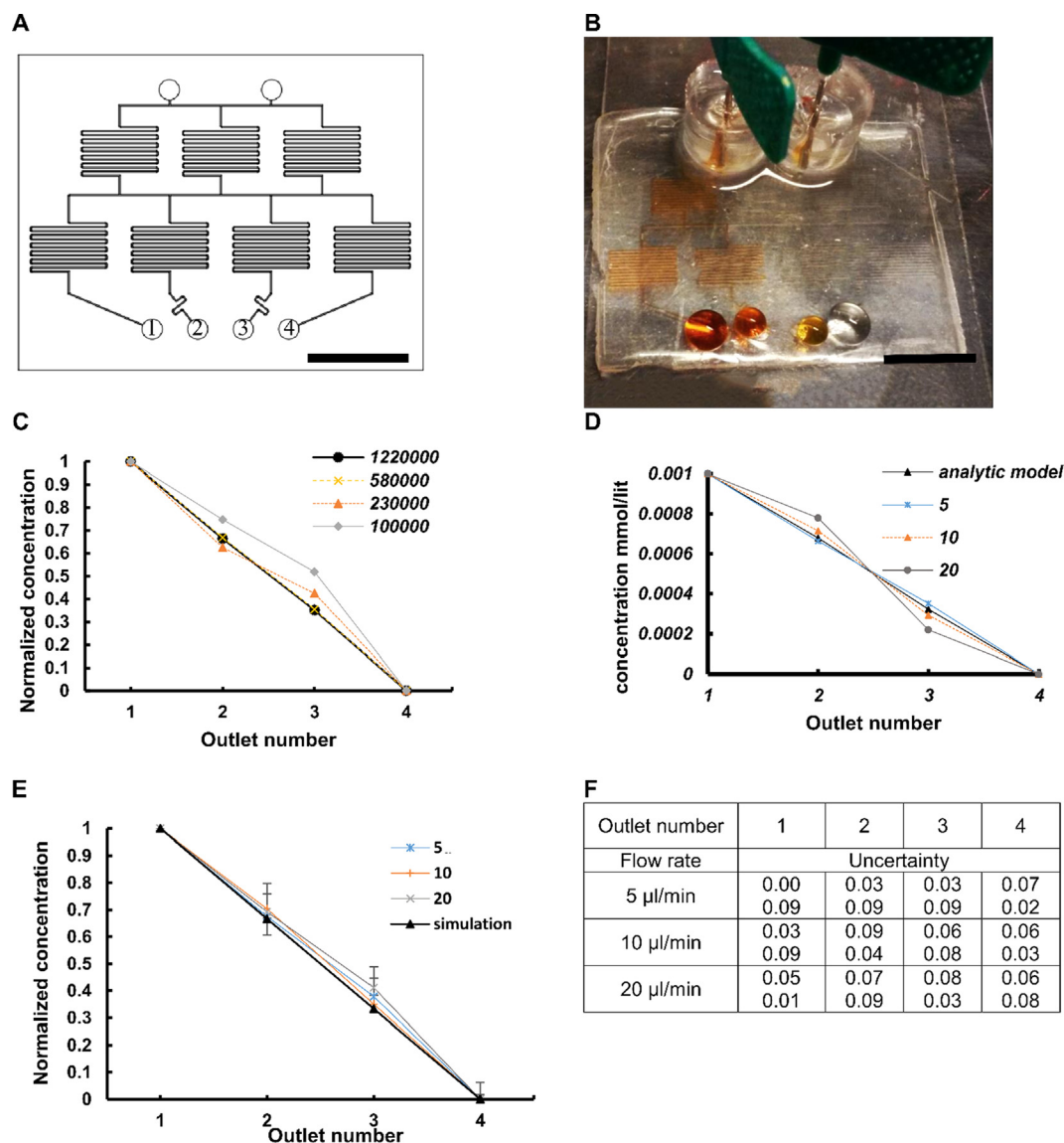
Fig. 2. (A) The shape of the designed mold (Scale bar: 10 mm). (B) The fabricated device. Red food dye was used in the channel, and a needle was used to inject the flow to the device (Scale bar: 10 mm). (C) Grid study of the simulation for a flow rate of 5 μl/min. The numbers under the horizontal axis are the outlet numbers shown in Fig. 2A. (D) Simulation of the device performance for different flow rates. (The unit of the numbers in the legend is in μl/min). The term "analytic model" refers to the corrected form of Eq. (4) based on the concentration outputs that the device was designed to generate. (E) Experimental colorimetric results of the output concentration. The error bars represent the test result range. The outlet numbers are mentioned in Fig. 2A. (The unit of the numbers in the legend is μl/min) (F) The values of the error bars in Fig. 2E. (For interpretation of the references to color in this figure legend, the reader is referred to the web version of this article.)

5 μl/min. The output concentration in the flow range of the design is linear; however, by increasing the flow rate, the concentration profile deviates from linearity. As mentioned before, this effect is due to the incomplete mixing that occurs in the presence of the high flow rate within the mixers. To investigate the reproducibility of the tests, all experiments were conducted three times, and the data are shown with error bars in Fig. 2E.

3.2. Second case – eight-output concentration device

The second CGG studied in this research is the eight-concentration single-drug device. This device mold was fabricated using CNC micromilling. The device was designed using the TCDT and was simulated using a CFD code. The resulted concentration of the device was evaluated using fluorescent emission intensity measurement.

3.2.1. Simulation results

Fig. 3A shows the device design. The large dimensions of the device (55 mm × 50 mm) are due to its high flow rate and the fabrication method. The device was designed based on the flow rate of 5 μl/min for each output and eight concentrations that resulted in a total amount of 40 μl/min. To improve the fluorescence imaging of the device, eight reservoirs were placed after each outlet of the device. The oblique placement of the channels is for reducing the width of the device because in this configuration, the mixers can be placed closer to each other (Fig. 3A).

As shown in Fig. 3A, the mixer length decreases as the liquid flows downstream in each stage of the device. This occurs because the number of mixers increases and the flow rate decreases in the mixers in the last stages. This effect was considered in the TCDT to keep the device dimensions as small as possible. In this device, the first stage mixer is 3.5 times longer than the last stage.
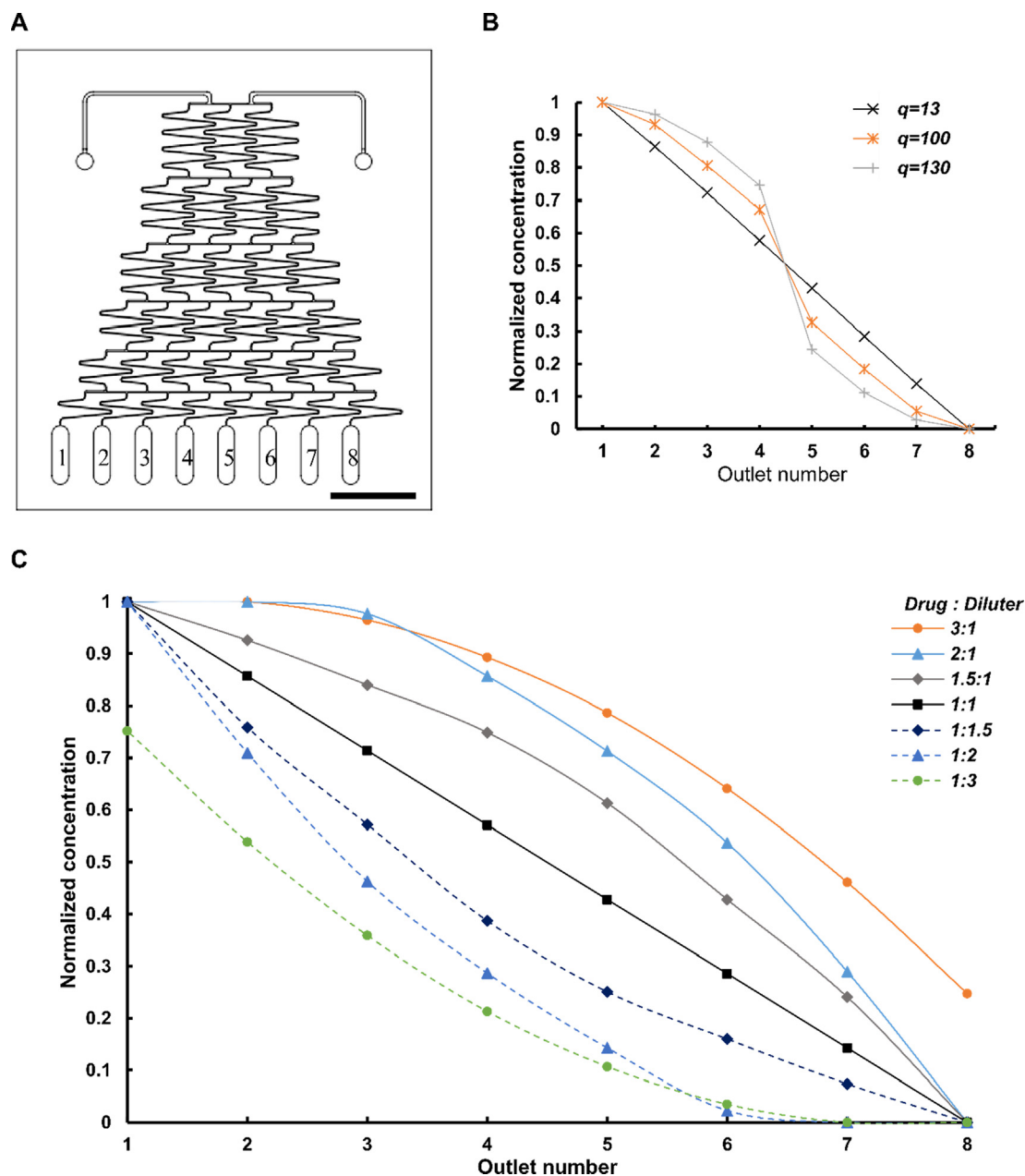
A

B

C

Fig. 3. (A) The schematic of the mold (Scale bar: 10 mm). (B) CFD results of the device performance in terms of normalized drug concentration for different flow rates at the outlets (outlet numbers are shown in (A)). (The unit of the numbers in the legend is µl/min). (C) Normalized concentration for different flow rate ratios of drug to diluter at the inlets, obtained by CFD simulation.

Fig. 3B depicts the CFD simulation results of the output concentrations for different flow rates. Increasing the flow rate to by one order of magnitude led to a reduction in the mixing performance. Increasing the flow rate in the channel does not allow enough time for diffusion before exiting the mixing channel. This effect is of utmost importance in the design of the mixers. Therefore, the length and the dimensions of mixers should be designed according to the flow rates within the channels to allow complete mixing, Eq. (4).

Most CGGs produce linear concentration gradients of drug. However, linear concentration gradients do not necessarily lead to the desired results. Non-linear concentrations are sometimes more beneficial because a small changes in drug quantity can result in a considerable change in concentration, particularly with a small concentration. Conversely, small changes may not have sensible changes for high drug concentrations (Toh et al., 2014).

Therefore, nonlinear output concentration leads to more comprehensive concentration change for effective drug screening.

TREE-LIKE CGGs can produce nonlinear concentration gradients by changing the ratio of the flow rate of the input fluids (Toh et al., 2014). The predicted nonlinear concentration profile in TREE-LIKE CGGs can be obtained more precisely if the number of the outputs is high enough (Keenan and Folch, 2008). Fig. 3C illustrates the response of the device predicted by the TCDT for different ratios of the flow rate in the input. By increasing the flow rate ratio to 3, the output concentration of the outlets nearest to the high flow rate input (e.g., outlet number 8 and 7 for 1:3 drug to diluter ratio) approaches the concentration of the higher flow rate. There is no outlet delivering the fluid with lower flow rate purely. Therefore, its highest normalized concentration is 0.75 (Fig. 3C). The nonlinear concentration output has a sharper gradient than the linear one. For example, for the diluter to drug flow rate ratio of 1.9,

the normalized drug concentrations are shown in Fig. 4A. By comparing the concentrations of the outlets of non-linear experiment to linear experiment (all except 1:1 to 1:1 in Fig. 3C or nonlinear ones to linear), it can be seen that by this combination of the drug and the diluter, a broader resolution of drug is provided. Especially for low concentrations at which small changes lead to large differences. To present the difference better, each output concentration was divided to the next one (concentration of outlet number 3 divided to number 2, number 4 divided to number 3, and so on). As shown in Fig. 4A for 1:1 and 1:1.9 of Rhodamine-B to diluter, the concentration ratios of the nonlinear combination provides a wider range of concentration ratios because it changes almost an order of magnitude (6 times) in the third outlet relative to the second. Therefore, this combination could be used for drug research more effectively as its range of concentration changes is more comprehensive.

3.2.2. Experimental performance analysis

One of the capabilities of TREE-LIKE CGGs is producing a variety of concentrations. In these devices, the performance is dependent on the pressure drop and the resistance of the channels. That means, any change in the resistance results into a change in the output flow rate and concentration distribution amongst the outlets of the device. Thus, it is highly critical to design and manufacture the channels and the downstream chip that delivers the output fluid of the device such that the pressure drop remains equal among parallel channels. The undesired outlet will be closed to use a smaller number of outlets. For example, if one of the
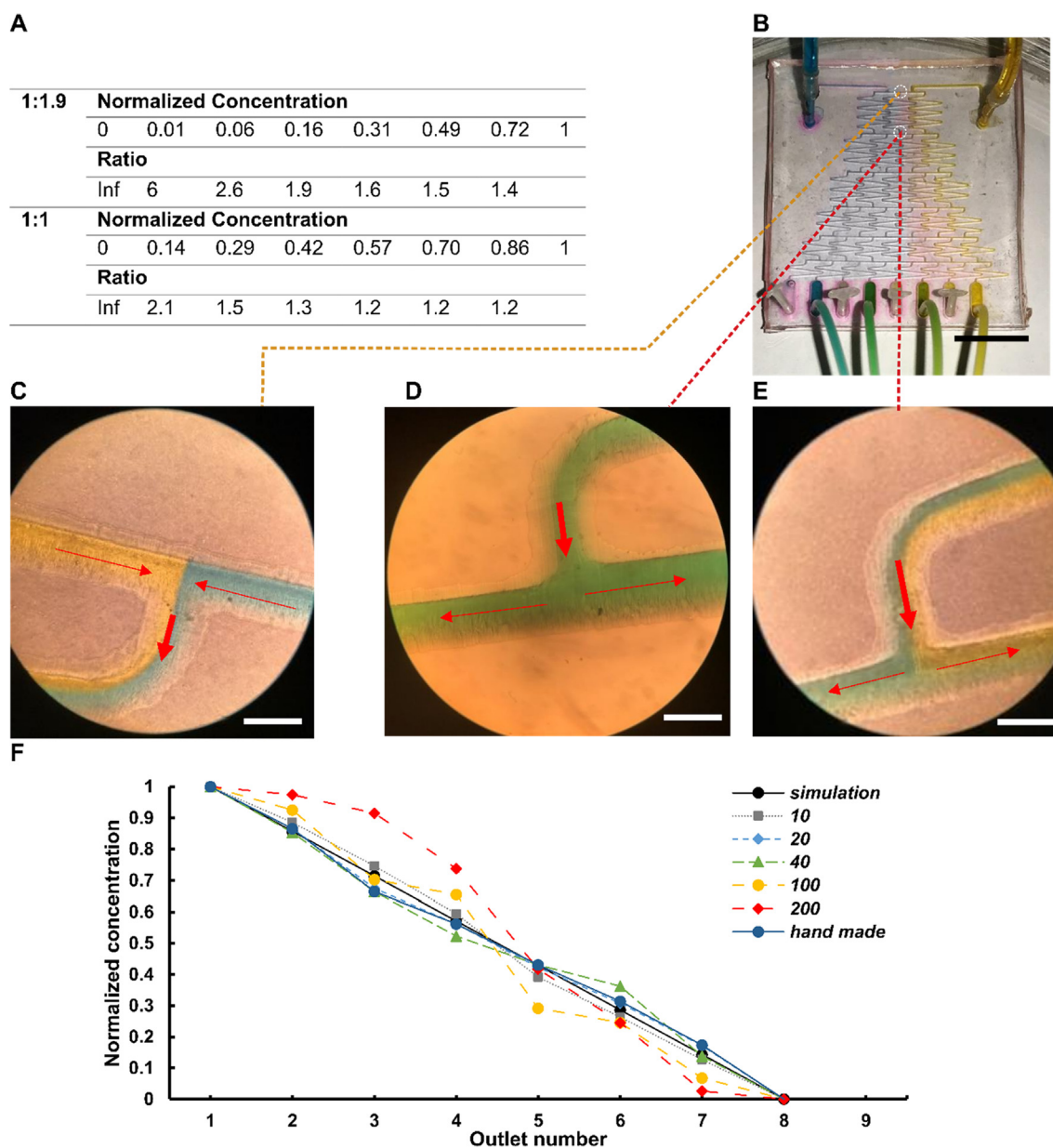

1:1.9	Normalized Concentration							
	0	0.01	0.06	0.16	0.31	0.49	0.72	1
	Ratio							
	Inf	6	2.6	1.9	1.6	1.5	1.4	
1:1	Normalized Concentration							
	0	0.14	0.29	0.42	0.57	0.70	0.86	1
	Ratio							
	Inf	2.1	1.5	1.3	1.2	1.2	1.2	

Fig. 4. (A) The output concentration and its ratio for flow ratio of Rhodamine-B to diluter 1:1.9 and 1:1 (B) Connection of the CGG for 4 output concentrations (Scale bar: 10 mm). (C) The inlet junction of the first mixer of the device; the interface between the streams is noticeable. The arrows indicate the flow direction (Scale bar: 0.15 mm) (D) The outlet of the first mixer of the device; the border vanishes due to complete mixing. (Arrows show the flow direction) (Scale bar: 0.15 mm). (E) The outlet of the first mixer of the device; the interface has not vanished due to incomplete mixing. The arrows indicate the flow direction (Scale bar: 0.15 mm) (F) The output concentration of the device for different flow rates in the experiment, the simulation, and the fabricated CGG. As the flow rate increases, the output concentration is less accurate (The error bars are omitted to allow visibility of all points) (The unit of the numbers in the legend is μl/min).

outlets is closed, the device will act exactly similar to a 7-outlet device. This effect was investigated in connection with a cell culture chip depicted in Fig. 4B. As can be seen, the device has created the desired color concentrations in both cases.

As mentioned above, the most crucial part of designing a CGG is the mixer. The inlet and outlet of a mixer are shown in Fig. 4C and D, respectively. At the inlet of the mixer, the two parallel flows are not mixed and have a visible interface. However, the interface vanishes, and mixing occurs completely downstream. As can be seen in Fig. 4C and D, the roughness on the channel wall created during fabrication of the mold, although not initially considered as a design parameter, improves the function of the device as it enhances mixing. If the mixer does not work perfectly, the interface between the streams does not vanish at the exit (Fig. 4E).

Two experiments were performed to measure the effect of changing the flow rate on the generation of linear and nonlinear concentrations. The fabricated device was connected to a syringe pump, and the output concentration was evaluated using fluorescence intensity measurement for different flow rates. By inducing the same flow rate of Rhodamine-B and water, the output concentration was linear for the inlet flow rate of 20 μl/min at each inlet of the CGG. For a higher discharge, the resulting concentration will slightly deviate from the desired value. For this test, the flow rate was set at 10, 20, 40, 100, 200 μl/min at each inlet, and the results of the light intensity of the fluorescence material are shown in Fig. 4F.

As shown in Fig. 4F, the device operates with an error as low as 5% up to the designed discharge of 20 μl/min at each inlet, but at a higher discharge, the result slightly deviates from the ideal (i.e. linear) concentration gradient. This effect was similarly predicted by the simulation shown in Fig. 4F. However, the deviation in the simulation was slightly lower than the experimental one, which was possibly due to the limitations in the fabrication accuracy as well as small bubbles trapped in the device. Bubbles will change the pressure drop in the channels that affect the flow rates. For instance, at very small flow rates, there is a slight deviation from
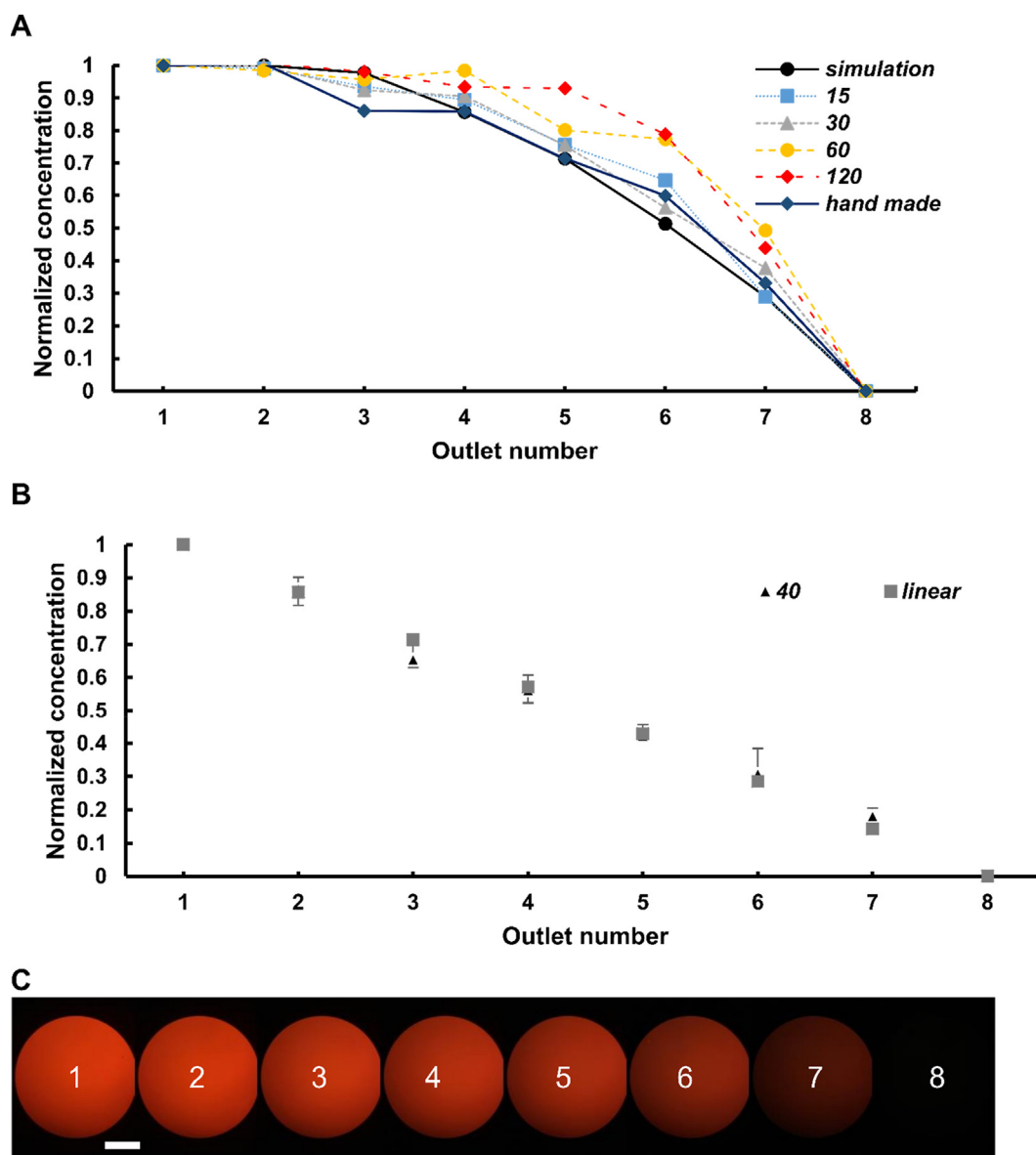

Fig. 5. (A) The output concentration of the device with the Rhodamine-B: water flow rate ratio of 2:1 for different flow rates. (Numbers in the legend are in μl/min) (B) The output concentration of the device for a flow rate of 40 μl/min. (The range of the results of the three experiments is shown as the uncertainty bars) (The unit of the numbers in the legend is μl/min). (C) The images captured from the CGG outlets with fluorescence microscopy (Scale bar: 0.05 mm).

the desired value due to the small pressure drop, and because there are some bubbles in the channels that result in unequal pressure drop between the parallel channels and altered output concentration.

The second experiment was designed to examine the effect of the difference in flow rates at the inlets on the device inputs. In this test, the flow rate of one of the inputs is two times larger than the flow rate at the other input. As obtained from the simulations shown in Fig. 5A, by changing the relative flow rate of the inputs of the device, the distribution of the concentration gradient at the outlet varies from linear to nonlinear with a sharper gradient. This effect is caused by the asymmetry created at the entrance, and consequently, in all channels. To perform this test, Rhodamine-B was used with the same concentration as in the first test. Rhodamine-B flow rate was twice as much as water's, and imaging took place under steady-state conditions. Normalized concentration graphs are shown in Fig. 5A.

With increasing ratios of Rhodamine-B to water flow rate at the inputs, the concentrations of the outlets near the rhodamine-B side increase and approach each other (Fig. 5A). This feature is especially useful for drug studies that do not specify a concentration level, as it can be used to test a greater range of concentrations and observe the effects. Increasing the input flow rate disrupts

the diffusion effect of the channels. This effect causes a great difference in the output concentration, similar to the linear concentration. Fig. 5B shows the results of the test performed for a flow rate of 40 μl/min. The images of the outlets are shown in Fig. 5C. The error bars are smaller at lower Rhodamine-B concentrations, which shows that the optical noises are less for small Rhodamine-B concentrations. In addition, as the data are normalized relative to the first and last output concentrations, the error bars are omitted in outlets 1 and 8.

3.3. Third case – Multi-drug chip

The multi-drug chip was designed using the TCDT for a flow rate of 15 μl/min from each inlet and diffusion coefficient of 5×10^{-10} m^2/s. The channel cross-section dimensions are 50×50 μm. The device was simulated using the CFD code and manufactured using a photolithographic mold and soft lithography. The output concentration of the device was measured using fluorescence emission measurement and color measurement.

The device has three inlets in the center and twelve outlets around the chip (Fig. 6A). This orientation of the mixers facilitates the investigation of the effect of three drugs. Fig. 6B illustrates the qualitative concentration distribution using food dyes at the
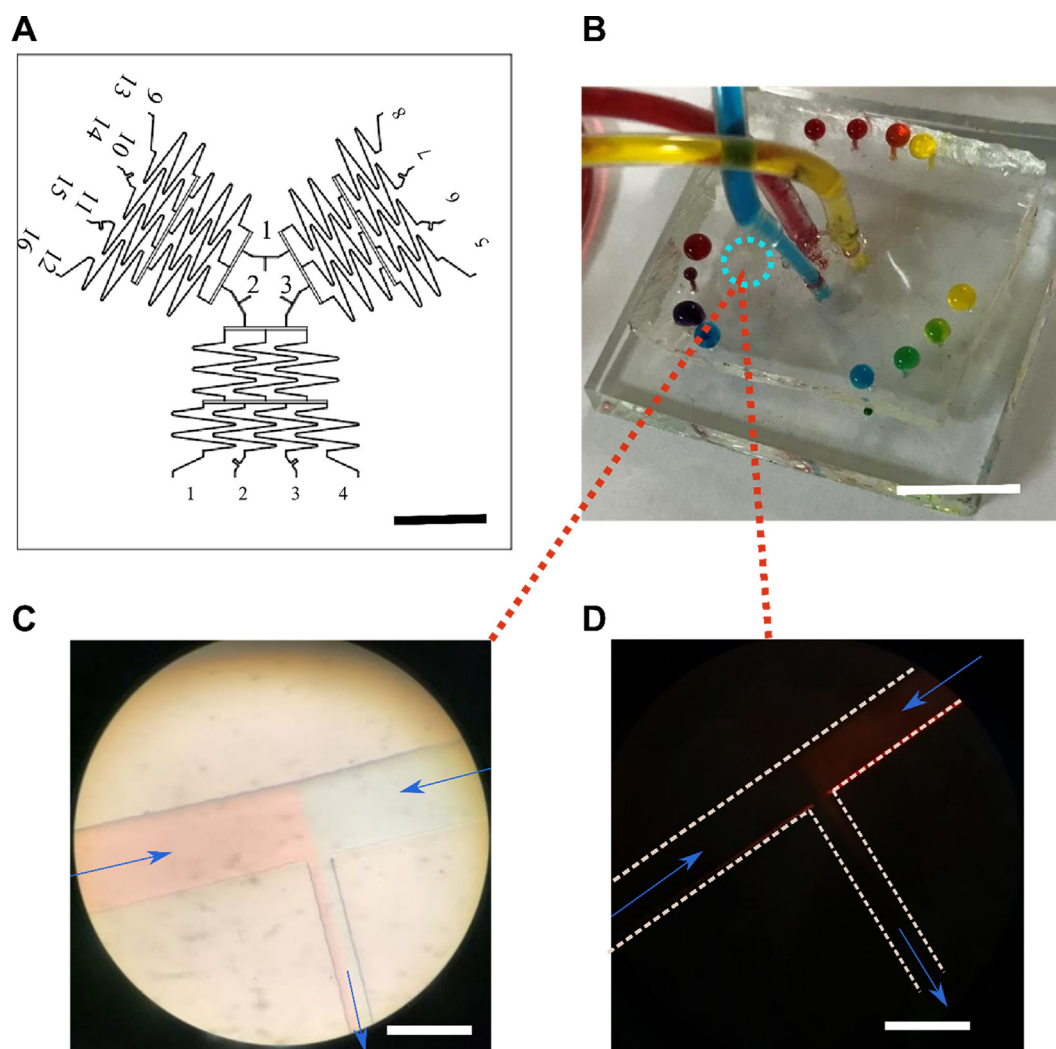

Fig. 6. (A) Overal schematic of the device's mold (scale bar: 10 mm). (B) The color gradient at the device outlets (Scale bar: 10 mm) (C & D) The inlet of the first mixer of the device visualized using food dye and fluorescent emission. (The white dashed lines represent the edge of the channels) (Arrows show the direction of flow) (Scale bars: 0.15 mm).

outlets. Fig. 6C and D show the inlet of the same mixer for color (C) and Rhodamine-B (D); the interface between the two streams is visible in both pictures.

3.3.1. Multi-drug multi-concentration method

In Fig. 7A, B and C, the output concentration of the device for a single drug, two drugs, and three drugs were investigated. Using this device with two drugs, the effects of each drug individually, as well as the two drugs simultaneously could be checked. By adding a third drug, it is not possible to check the function of the drugs individually. In contrast, the two-by-two interactions of the three drugs are examined.

Fig. 7A, B and C show the simulated output concentrations of the device for the design flow rate. Fig. 7A is the output concentration of the device for a single drug from one inlet and diluter from two inlets. This combination does not have any

new features compared to the single-drug chip. Fig. 7B shows the results of adding two drugs from two inlets (no matter which one) and the diluter from the third one. This combination can produce the concentration gradient of two drugs with diluter (outlets 5–8 and 9–12) and the combination of the two drugs (outlets 1–4). Using this method, it is possible to compare the effect of two drugs with a single drug. Fig. 7C demonstrates the two-by-two combination of three drugs. With this method, the effect of the drug combinations (outputs 2, 3, 6, 7, 10, and 11) and also single drug effect (outputs 1, 4, 5, 8, 9, 12) can be examined. This device allows for finding the best combination of the drugs first. Subsequently, the single-drug chip finds the best concentration of the drugs. In addition, this device can be used to investigate the effect of two-by-two combinations of three drugs relative to each other and find the best drug concentration using the single-drug chip.
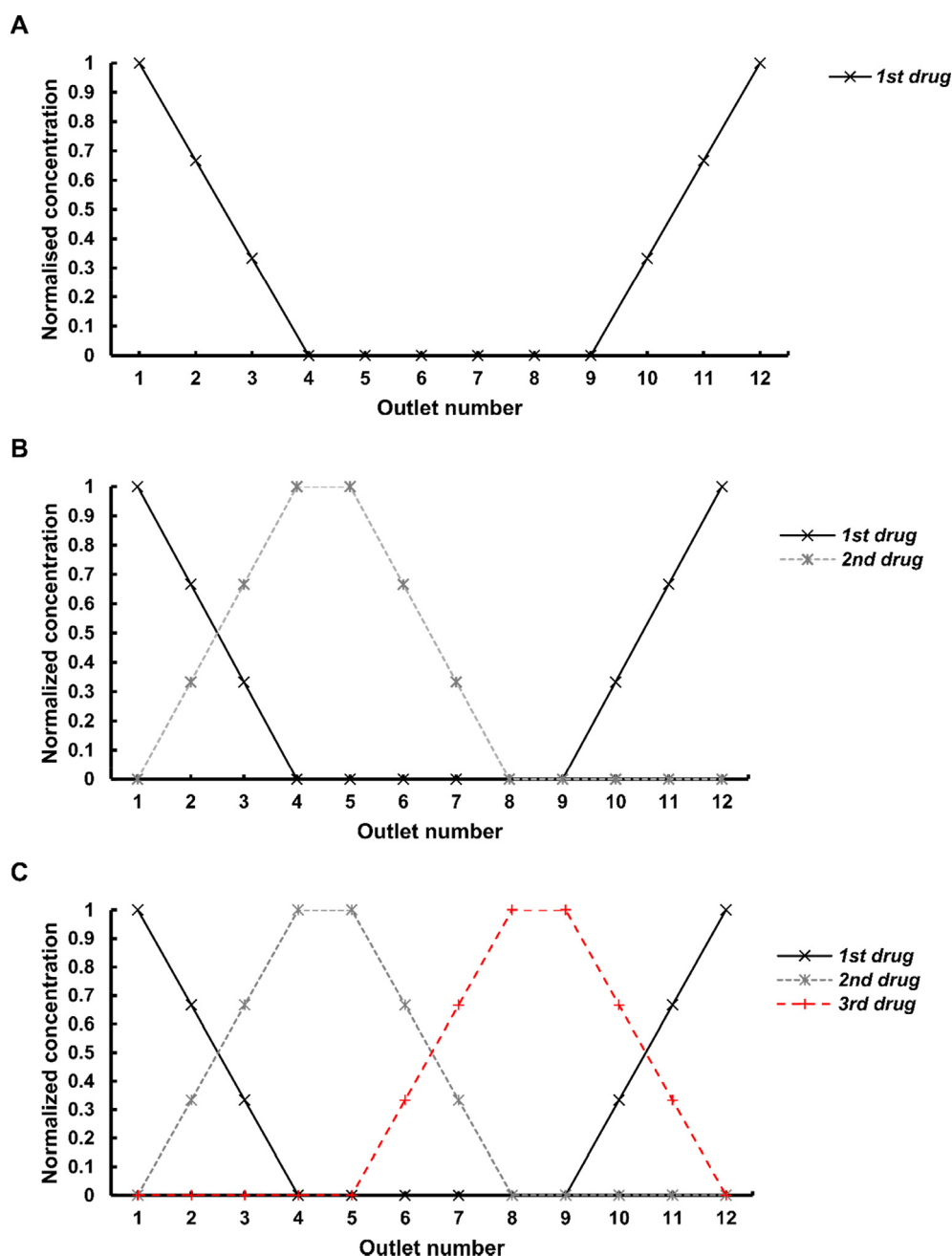

Fig. 7. Simulation results of the device (A) One-drug. (B)Two-drugs. (C) Three-drugs.

The method mentioned above is called *Multi-Drug Multi-Concentration chip* (MDMC) for personalized medicine. MDMC on a patient could be an off-the-shelf (Mark et al., 2012) personalized medicine approach for patients with more than a single drug option. The method is based on the fact that for each person and drug combination, there is a need for designing a specific CGG based on the requirements mentioned before. Thus, using the TCDT and the MDMC method together can produce the desired results applicable in personalized medicine, especially because it is compatible with the low-cost rapid prototyping methods such as 3D printing.

3.3.2. Experimental performance analysis

Because there are three different inputs in the multi-drug sample, Rhodamine-B and distilled water are not adequate for the performance analysis. The experiment was divided into two stages. In the first stage, the fluorescence material in one of the inlets such as inlet 2 and the diluter in the other two inlets entered the device (Fig. 8A), and concentration gradient formed in two sections of the three sections (outlets 1–4, 13–16 in Fig. 8A). In the second stage, by changing the device inputs (Rhodamin-B in inlet 1 and water in 2&3), the concentration gradient was formed in the third section (outlets 5–8) as well as outlets 9–12 (Fig. 8B), which were examined in stage 1 as 13–16. Fig. 8C shows the generated concentrations.

Comparing the two stages of examination and normalizing the data could measure the concentration gradient of the device, Fig. 8C. In Fig. 8C, outlets 13–16 represent outlets 12–9 respectively in the second stage of the experiment and the concentrations of the outlets 5–8 are equal to those of the second stage. This experiment was designed to validate the mixing performance at a flow rate of 15 µl/min. As illustrated, all the mixers have the same performance and react the same in the measurement of Rhodamine-B emission.

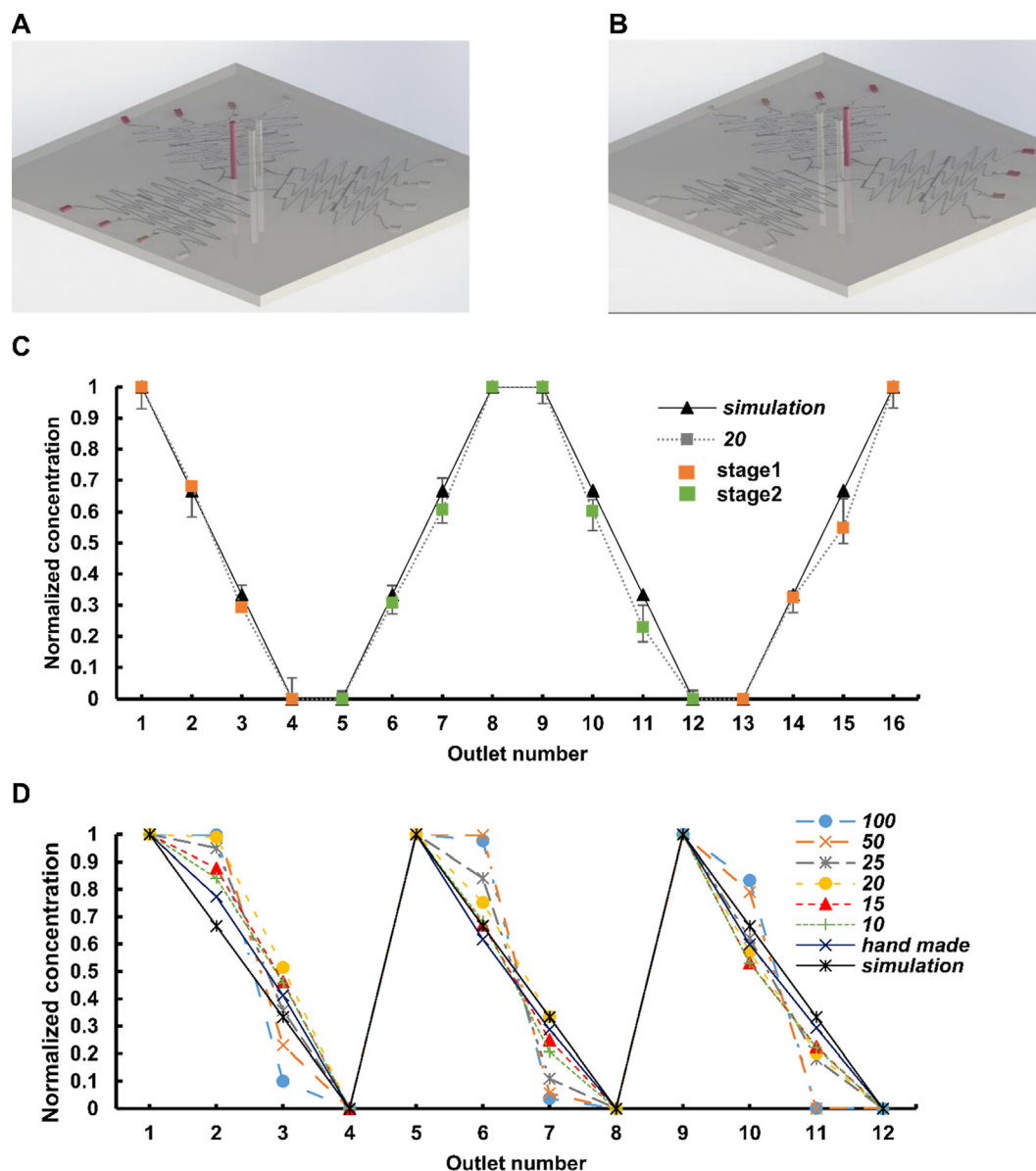The above method is suitable for measuring the single concentration gradient, which was used to examine the mixing

Fig. 8. (A&B) The first stage and the second stage of the experiment. (C) The output concentration of the device for the flow rate of 20 µl/min using fluorescence emission measurement. The error bars are the range of the three experiments. (The numbers are represented in Fig. 7A) (The unit of the numbers in the legend is µl/min) (D) The output concentration of the device using colorimetric method (The unit of the numbers in the legend is µl/min).

performance. The concentration was measured based on food dye intensity to determine the threshold flow rate below which the device output concentration remains unaffected. Food dye measurement makes it possible to investigate the CGG performance when more than two inputs with various drugs exist. For this purpose, the HSV method for color processing was used. Three colors, red, yellow, and blue, were introduced to the device. Because at each outlet, the color was a combination of two colors, e.g., red and blue, the relative color of each outlet was measured. Fig. 8D depicts the concentration in each outlet are as follows: outlets 1–4, concentrations of red compared with blue, outlets 5–8 concentrations of blue in comparison with yellow, and outlets 9–12, concentrations of red in comparison with yellow.

Finally, the performance of the device at different flow rates was evaluated. Simulation results are compared with experimental data in Fig. 8D. The experimental output and the simulated output agree well for the design flow rate of 15 μl/min at each inlet. However, increasing the flow rate leads to discrepancy between simulation and experiment. As mentioned above, this effect is due to incomplete diffusion resulting from the high flow rate. A critical feature in this device is that it was more sensitive to flow rate change than others represented before. A small increase in the flow rate above the designed values (from 15 to 25 μl/min), the mixing performance decreases rapidly (by more than 20%). This effect is caused by the smoothing of the sharp edges of the channel when the device mold was made using photolithography techniques. In the micromachining and stereolithography techniques, the channel edges were not sharp and had some roughness. The roughness enhances mixing and improves the performance of the device. With photolithography, well-defined edges and smooth channel walls hinder convective mixing and increase the required mixing length.

4. Conclusion

This paper reports a design tool for CGGs. Three different cases were fabricated using the TCDT, and their performance was evaluated experimentally and numerically. TCDT is useful for designing the CGGs made by micromachining, photolithography, and 3D printing. The tool can calculate the dimensions required for making a regular CGG with a number of outlets and non-linear output concentration. In order to validate the model in terms of the fabrication method and the repeatability of the output concentration, the output concentrations were measured using Rhodamine-B and food dye for three different chip designs. The TCDT code can be modified to customize the design of the TREE-LIKE CGGs for various lab-on-a-chip applications. The proposed design tool can provide more precise results and a straightforward procedure for CGGs. This tool is placed in the public domain as open-source code. Furthermore, the MDMC method was presented. This method can find the best drug combinations using the multi-drug device, and then using the single-drug device, the best drug concentration of that combination can be found. Based on the fact that non-linear concentration gradients can better investigate the drug concentration changes in dilute solutions, the TCDT can calculate the related calculations and be used in MDMC method.

Declaration of Competing Interest

The authors declare no conflicts of interest.

Appendix A. Supplementary material

Supplementary data to this article can be found online at https://doi.org/10.1016/j.ces.2019.115339.

References

Abhyankar, V.V., Lokuta, M.A., Huttenlocher, A., Beebe, D.J., 2006. Characterization of a membrane-based gradient generator for use in cell-signaling studies. Lab Chip 6, 389–393.

Boyden, S., 1962. The chemotactic effect of mixtures of antibody and antigen on polymorphonuclear leucocytes. J. Exp. Med. 115, 453–466.

Bui, M.-P.N., Li, C.A., Han, K.N., Choo, J., Lee, E.K., Seong, G.H., 2011. Enzyme kinetic measurements using a droplet-based microfluidic system with a concentration gradient. Anal. Chem. 83, 1603–1608.

Çengel, Y.A., 2010. Fluid Mechanics. Tata McGraw Hill Education Private.

Chang, C.-W., Cheng, Y.-J., Tu, M., Chen, Y.-H., Peng, C.-C., Liao, W.-H., Tung, Y.-C., 2014a. A polydimethylsiloxane–polycarbonate hybrid microfluidic device capable of generating perpendicular chemical and oxygen gradients for cell culture studies. Lab Chip 14, 3762–3772.

Chang, T.C., Mikheev, A.M., Huynh, W., Monnat, R.J., Rostomily, R.C., Folch, A., 2014b. Parallel microfluidic chemosensitivity testing on individual slice cultures. Lab Chip 14, 4540–4551.

Chiang, H.-C., Wang, Y.-S., Chou, C.-H., Liao, A.T., Chu, R.-M., Lin, C.-S., 2012. Overexpression of chemokine ligand 7 is associated with the progression of canine transmissible venereal tumor. BMC Vet. Res. 8, 216.

Chung, B.G., Flanagan, L.A., Rhee, S.W., Schwartz, P.H., Lee, A.P., Monuki, E.S., Jeon, N.L., 2005. Human neural stem cell growth and differentiation in a gradient-generating microfluidic device. Lab Chip 5, 401–406.

Crank, J., 1979. The Mathematics of Diffusion. Clarendon Press.

Diao, J., Young, L., Kim, S., Fogarty, E.A., Heilman, S.M., Zhou, P., Shuler, M.L., Wu, M., DeLisa, M.P., 2006. A three-channel microfluidic device for generating static linear gradients and its application to the quantitative analysis of bacterial chemotaxis. Lab Chip 6, 381–388.

DiCicco, M., Neethirajan, S., 2014. An in vitro microfluidic gradient generator platform for antimicrobial testing. Biochip J. 8, 282–288.

Gao, Y., Sun, J., Lin, W.-H., Webb, D.J., Li, D., 2012. A compact microfluidic gradient generator using passive pumping. Microfluid. Nanofluid. 12, 887–895.

Gendron, P.-O., Avaltroni, F., Wilkinson, K.J., 2008. Diffusion coefficients of several rhodamine derivatives as determined by pulsed field gradient-nuclear magnetic resonance and fluorescence correlation spectroscopy. J. Fluorescence 18, 1093.

Girod, B., Niemann, H., Seidel, H.P., 1999. Vision Modelling and Visualization '99. IOS Press, Incorporated.

Glawdel, T., Elbuken, C., Lee, L.E., Ren, C.L., 2009. Microfluidic system with integrated electroosmotic pumps, concentration gradient generator and fish cell line (RTgill-W1)—towards water toxicity testing. Lab Chip 9, 3243–3250.

Gundersen, R., Barrett, J., 1979. Neuronal chemotaxis: chick dorsal-root axons turn toward high concentrations of nerve growth factor. Science 206, 1079–1080.

Harrison, H., Lu, X., Patel, S., Thomas, C., Todd, A., Johnson, M., Raval, Y., Tzeng, T.-R., Song, Y., Wang, J., Li, D., Xuan, X., 2015. Electrokinetic preconcentration of particles and cells in microfluidic reservoirs. Analyst 140, 2869–2875.

Heo, Y., Cabrera, L., Bormann, C., Shah, C., Takayama, S., Smith, G., 2010. Dynamic microfunnel culture enhances mouse embryo development and pregnancy rates. Hum. Reprod. 25, 613–622.

Hong, B., Xue, P., Wu, Y., Bao, J., Chuah, Y.J., Kang, Y., 2016. A concentration gradient generator on a paper-based microfluidic chip coupled with cell culture microarray for high-throughput drug screening. Biomed. Microdevices 18, 21.

Hu, C., Liu, J., Chen, H., Nie, F., 2017. Microfluidic platforms for gradient generation and its applications. Biochem. Anal. Biochem. 6 (2161–1009), 1000320.

Huang, C.-H., Hou, H.-S., Lo, K.-Y., Cheng, J.-Y., Sun, Y.-S., 2017. Use microfluidic chips to study the effects of ultraviolet lights on human fibroblasts. Microfluid. Nanofluid. 21, 79.

Integra_support, 2017. Serial dilution using 96/384-channel pipette, facrory user manual, p. 21.

Jain, M., Yeung, A., Nandakumar, K., 2010. Induced charge electro-osmotic concentration gradient generator. Biomicrofluidics 4. 014110.

Jang, Y.-H., Hancock, M.J., Kim, S.B., Selimovic, S., Sim, W.Y., Bae, H., Khademhosseini, A., 2011. An integrated microfluidic device for two-dimensional combinatorial dilution. Lab Chip 11, 3277–3286.

Jeon, N.L., Baskaran, H., Dertinger, S.K., Whitesides, G.M., Van De Water, L., Toner, M., 2002. Neutrophil chemotaxis in linear and complex gradients of interleukin-8 formed in a microfabricated device. Nat. Biotechnol. 20, 826–830.

Jeon, N.L., Dertinger, S.K., Chiu, D.T., Choi, I.S., Stroock, A.D., Whitesides, G.M., 2000. Generation of solution and surface gradients using microfluidic systems. Langmuir 16, 8311–8316.

Jin, D., Ma, X., Luo, Y., Fang, S., Xie, Z., Li, X., Qi, D., Zhang, F., Kong, J., Li, J., 2016. Application of a microfluidic-based perivascular tumor model for testing drug sensitivity in head and neck cancers and toxicity in endothelium. RSC Adv. 6, 29598–29607.

Joanne Wang, C., Li, X., Lin, B., Shim, S., Ming, G.-L., Levchenko, A., 2008. A microfluidics-based turning assay reveals complex growth cone responses to integrated gradients of substrate-bound ECM molecules and diffusible guidance cues. Lab Chip 8, 227–237.

Kashaninejad, N., Nikmaneshi, M.R., Moghadas, H., Kiyoumarsi Oskouei, A., Rismanian, M., Barisam, M., Saidi, M.S., Firoozabadi, B., 2016. Organ-tumor-on-a-chip for chemosensitivity assay: a critical review. Micromachines 7, 130.

Keenan, T.M., Folch, A., 2008. Biomolecular gradients in cell culture systems. Lab Chip 8, 34–57.

Kendig, S., 2003. Use of microchannels to determine diffusion of food coloring in water. Microelectronics Processing Technology Fall Term.

Kilinc, D., Schwab, J., Rampini, S., Ikpekha, O.W., Thampi, A., Blasiak, A., Li, P., Schwamborn, R., Kolch, W., Matallanas, D., Lee, G.U., 2016. A microfluidic dual gradient generator for conducting cell-based drug combination assays. Integr. Biol. 8, 39–49.

Kothapalli, C.R., van Veen, E., de Valence, S., Chung, S., Zervantonakis, I.K., Gertler, F.B., Kamm, R.D., 2011. A high-throughput microfluidic assay to study neurite response to growth factor gradients. Lab Chip 11, 497–507.

Kwapiszewska, K., Żukowski, K., Kwapiszewski, R., Brzózka, Z., 2016. Double casting prototyping with a thermal aging step for fabrication of 3D microstructures in poly (dimethylsiloxane). AIMS Biophys. 3, 553–562.

Lee, J.M., Kim, J.-E., Kang, E., Lee, S.-H., Chung, B.G., 2011. An integrated microfluidic culture device to regulate endothelial cell differentiation from embryonic stem cells. Electrophoresis 32, 3133–3137.

Lee, K., Kim, C., Jung, G., Kim, T.S., Kang, J.Y., Oh, K.W., 2010. Microfluidic network-based combinatorial dilution device for high throughput screening and optimization. Microfluid. Nanofluid. 8, 677–685.

Ligrani, P.M., 1994. A study of Dean vortex development and structure in a curved rectangular channel with aspect ratio of 40 at Dean numbers up to 430.

Lim, W., Park, S., 2018. A microfluidic spheroid culture device with a concentration gradient generator for high-throughput screening of drug efficacy. Molecules 23, 3355.

Lin, F., Saadi, W., Rhee, S.W., Wang, S.-J., Mittal, S., Jeon, N.L., 2004. Generation of dynamic temporal and spatial concentration gradients using microfluidic devices. Lab Chip 4, 164–167.

Liu, M.C., Ho, D., Tai, Y.-C., 2008. Monolithic fabrication of three-dimensional microfluidic networks for constructing cell culture array with an integrated combinatorial mixer. Sens. Actuators, B 129, 826–833.

Liu, W., Ren, Y., Chen, F., Song, J., Tao, Y., Du, K., Wu, Q., 2019. A microscopic physical description of electrothermal-induced flow for control of ion current transport in microfluidics interfacing nanofluidics. Electrophoresis.

Mark, D., von Stetten, F., Zengerle, R., 2012. Microfluidic apps for off-the-shelf instruments. Lab Chip 12, 2464–2468.

Moshksayan, K., Kashaninejad, N., Saidi, M., 2018a. Inventions and innovations in preclinical platforms for cancer research. Inventions 3, 43.

Moshksayan, K., Kashaninejad, N., Warkiani, M.E., Lock, J.G., Moghadas, H., Firoozabadi, B., Saidi, M.S., Nguyen, N.-T., 2018b. Spheroids-on-a-chip: Recent advances and design considerations in microfluidic platforms for spheroid formation and culture. Sens. Actuators, B 263, 151–176.

Nguyen, B., Graham, P.J., Sinton, D., 2016. Dual gradients of light intensity and nutrient concentration for full-factorial mapping of photosynthetic productivity. Lab Chip 16, 2785–2790.

Nguyen, N.-T., 2012a. Chapter 2 - Fundamentals of Mass Transport in the Microscale, Micromixers (Second Edition). William Andrew Publishing, Oxford, pp. 9–72.

Nguyen, N.-T., 2012b. Chapter 9 - Application of Micromixers, Micromixers (Second Edition). William Andrew Publishing, Oxford, pp. 321–342.

Park, J.Y., Hwang, C.M., Lee, S.H., Lee, S.-H., 2007. Gradient generation by an osmotic pump and the behavior of human mesenchymal stem cells under the fetal bovine serum concentration gradient. Lab Chip 7, 1673–1680.

Python, 2019. Software Foundation, Python Language Reference, version 3.7

Ramesan, S., Rezk, A.R., Cheng, K.W., Chan, P.P., Yeo, L.Y., 2016. Acoustically-driven thread-based tuneable gradient generators. Lab Chip 16, 2820–2828.

Rao, S.S., 1996. Engineering Optimization. Wiley.

Ren, Y., Song, C., Liu, W., Jiang, T., Song, J., Wu, Q., Jiang, H., 2019. On hybrid electroosmotic kinetics for field-effect-reconfigurable nanoparticle trapping in a four-terminal spiral microelectrode array. Electrophoresis 40, 979–992.

Rismanian, M., Saidi, M.S., Kashaninejad, N., 2019. A new non-dimensional parameter to obtain the minimum mixing length in tree-like concentration gradient generators. Chem. Eng. Sci. 195, 120–126.

Ruppen, J., Wildhaber, F.D., Strub, C., Hall, S.R.R., Schmid, R.A., Geiser, T., Guenat, O.T., 2015. Towards personalized medicine: chemosensitivity assays of patient lung cancer cell spheroids in a perfused microfluidic platform. Lab Chip 15, 3076–3085.

Shames, I.H., 2003. Mechanics of Fluids. McGraw-Hill.

Toh, A.G., Wang, Z., Yang, C., Nguyen, N.-T., 2014. Engineering microfluidic concentration gradient generators for biological applications. Microfluid. Nanofluid. 16, 1–18.

Tretkoff, E., 2005. Building a Better Fuel Cell Using Microfluidics. APS news 14.

Truskey, G.A., Yuan, F., Katz, D.F., 2004. Transport phenomena in biological systems.

Walker, G.M., Sai, J., Richmond, A., Stremler, M., Chung, C.Y., Wikswo, J.P., 2005. Effects of flow and diffusion on chemotaxis studies in a microfabricated gradient generator. Lab Chip 5, 611–618.

Wang, F., 2009. The signaling mechanisms underlying cell polarity and chemotaxis. Cold Spring Harbor Perspectives in Biology 1.

Yang, C.-G., Wu, Y.-F., Xu, Z.-R., Wang, J.-H., 2011. A radial microfluidic concentration gradient generator with high-density channels for cell apoptosis assay. Lab Chip 11, 3305–3312.

Ye, N., Qin, J., Shi, W., Liu, X., Lin, B., 2007. Cell-based high content screening using an integrated microfluidic device. Lab Chip 7, 1696–1704.

Zicha, D., Dunn, G.A., Brown, A.F., 1991. A new direct-viewing chemotaxis chamber. J. Cell Sci. 99, 769–775.

Zigmond SH, H.J., 1973. Leukocyte locomotion and chemotaxis New methods for evaluation and demostration of a celldervice chemotactic factor. J. Exp. Med. 137, 23.